Wavefront sensorless adaptive optics for large aberrations

Martin J. Booth

Department of Engineering Science, University of Oxford, Parks Road, Oxford, OX1 3PJ, UK

Received August 30, 2006; revised September 27, 2006; accepted September 28, 2006;
posted October 5, 2006 (Doc. ID 74525); published December 13, 2006

In some adaptive optics systems the aberration is determined not by using a wavefront sensor but by sequential optimization of the adaptive correction element. Efficient schemes for the control of such systems are essential if they are to be effective. A scheme is introduced that permits the efficient measurement of large amplitude wavefront aberrations that are represented by an appropriate series of modes. This scheme uses an optimization metric based on the root-mean-square spot radius (or focal spot second moment) and an aberration expansion using polynomials suited to the representation of lateral aberrations. Experimental correction of N aberration modes is demonstrated with a minimum of $N+1$ photodetector measurements. The geometrical optics basis means that the scheme can be extended to arbitrarily large aberrations.

OCIS codes: 010.1080, 010.7350.

Several applications that benefit from adaptive optics do not necessarily require a wavefront sensor. These systems operate by the sequential reconfiguration of the adaptive correction element and the maximization of a feedback signal according to a particular optimization algorithm. Such systems have been demonstrated in, for example, intracavity aberration correction in lasers, optical trapping, free-space laser propagation, and microscopy. Many previous methods have employed stochastic, model-free, local or global search methods along with adaptive or empirical algorithm optimization. It has recently been shown that a model-based approach to such wavefront sensorless systems leads to efficient, deterministic algorithms.[1] However, this was limited to phase aberrations with root-mean-square (rms) amplitudes smaller than 1 rad. In this Letter this approach is extended, and a scheme that can be used for arbitrarily large aberrations is introduced.

It is well known that for small aberrations the Strehl intensity of a wavefront does not depend on the form of the aberration, but only on its variance.[2] If the input aberration $\Phi(r,\theta)$ is represented by a series of N orthonormal Zernike polynomials $Z_i(r,\theta)$, such that $\Phi=\Sigma_i a_i Z_i$, this Strehl intensity can be expressed simply as

$$S \approx 1 - |\mathbf{a}|^2, \tag{1}$$

where $\mathbf{a}$ is the N-element vector comprising the coefficients a_i. The Zernike polynomials are normalized such that $a_i=1$ is equivalent to a wavefront variance of 1 rad^2.[3] This normalization, along with the orthogonality of the Zernike polynomials, gives rise to the simple form of relation (1). If the vector $\mathbf{a}$ is considered to represent a point in N-dimensional space, then the contours of constant S form N-dimensional spheres. In addition to this spherical symmetry, S has a well-defined maximum at the origin and becomes small for large aberrations. Taking advantage of these properties, it has been shown that, by using a Strehl-based optimization metric, a combination of N Zernike modes could be measured by using $N+1$ photodetector measurements.[1] However, this approach relied on relationship (1), and consequently the maximum amplitude that could be reliably measured was limited to around 1 rad rms. This scheme used the system shown in Fig. 1(a), where the photodetector took the form of an on-axis pinhole whose diameter was much smaller than a diffraction-limited spot. However, when aberrations are large most of the light is directed away from the optical axis and the detector. For these larger aberrations the pointlike detector, the Strehl intensity optimization metric, and the Zernike polynomial representation of the aberration are no longer appropriate.

To extend this approach to larger aberrations, we require a function that has properties similar to S, namely, a distinct maximum and spherical symmetry, but one that maintains these properties over a larger range of aberration amplitudes. We therefore intro-

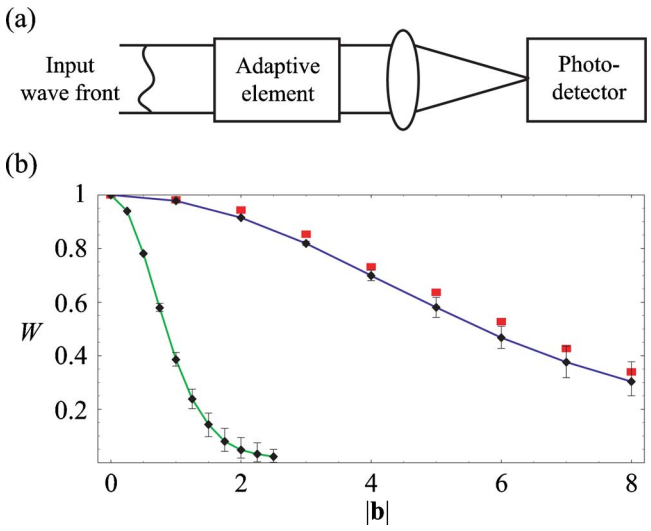

Fig. 1. (Color online) (a) Schematic of the optical system. (b) Normalized signal response, using LZ modes and quadratic detector (upper, blue curve), experimentally determined figures (red squares), pointlike detector and Zernike modes (lower, green curve).

duce a scheme that is based on the measurement of the rms spot radius and employs a larger detector with spatially varying sensitivity, a different optimization metric, and a more appropriate aberration representation. Rather than using the Zernike polynomials, we expand the aberration as a series of functions that more directly relate to the spot radius. These functions were first derived by Lukosz[4] and, later, independently by Braat.[5] Like Zernike polynomials, the Lukosz–Zernike (LZ) functions are each expressed as the product of a radial and azimuthal function using the same dual index and numbering scheme. They can be defined as

$$L_n^m(r,\theta) = B_n^m(r)\begin{cases}\cos(m\theta) & m \geq 0\\ \sin(m\theta) & m < 0\end{cases}, \tag{2}$$

where n and m are the radial and azimuthal indices, respectively, and where

$$B_n^m(r) = \begin{cases}\sqrt{\dfrac{1}{n}}[R_n^0(r) - R_{n-2}^0(r)] & m = 0\\ \sqrt{\dfrac{2}{n}}[R_n^m(r) - R_{n-2}^m(r)] & n \neq m \neq 0\\ \dfrac{2}{\sqrt{n}}R_n^n(r) & m = n \neq 0\end{cases}. \tag{3}$$

$R_n^m(r)$ is the Zernike radial polynomial given by

$$R_n^m(r) = \sum_{k=0}^{\frac{n-m}{2}} \frac{(-1)^k (n-k)!\, r^{n-2k}}{k!\left(\dfrac{n+m}{2}-k\right)!\left(\dfrac{n-m}{2}-k\right)!}. \tag{4}$$

The normalization in Eq. (3) has been chosen so that the contribution of each mode to the rms transverse aberration (or equivalently the rms spot radius) is independent of its indices (n,m). The phase aberration $\Phi = \Sigma_{n,m} b_{n,m} L_n^m$ gives a mean-square spot radius of

$$\langle \rho^2 \rangle = \left(\frac{\lambda}{\mathrm{NA}}\right)^2 \sum_{n,m} b_{n,m}^2 = \left(\frac{\lambda}{\mathrm{NA}}\right)^2 |\mathbf{b}|^2, \tag{5}$$

where λ is the wavelength, NA is the numerical aperture of the lens, and the elements of the vector $\mathbf{b}$ are the modal coefficients $b_{n,m}$. Whereas a Zernike polynomial of a given order is defined to minimize the rms value of the wavefront phase, the LZ polynomials are defined to minimize the rms spot radius. We therefore employ an intensity measurement that is related to the spot radius. For a large detector whose sensitivity D varies across its area, the detected signal is given by

$$W = \int_\nu \int_\xi I(\nu,\xi) D(\nu,\xi) \nu \, \mathrm{d}\nu \, \mathrm{d}\xi, \tag{6}$$

where (ν,ξ) are the polar coordinates in the detector plane and I is the focal spot intensity distribution, which is readily calculated, when one is modeling the system, by using the Fourier transform of the complex field in the lens pupil. The radial coordinate is normalized such that the first intensity zero of the diffraction-limited focal spot for a circular aperture lies at $\nu = 1.22\pi$. If the detector sensitivity is chosen such that $D = \nu^2$, then Eq. (6) is equivalent, in the geometrical optics regime, to a measurement of the mean-square spot radius (multiplied by total intensity). If we combined such a measurement with an aberration expansion in terms of the LZ polynomials, we would have a representation with the desired spherical symmetry. However, this representation provides a minimum, rather than a maximum, for zero aberration. Furthermore, in practice, we require that the detector be finite in extent. If instead we choose the quadratic sensitivity $D = (1 - \nu^2/R^2)$ for $\nu \leq R$ and zero otherwise, where R is a suitably chosen detector radius, we obtain a representation of W that has the desired properties. This leads to the relationship $W \approx 1 - c|\mathbf{b}|^2$, where c is a scalar that depends on R. Figure 1(b) shows the calculated response of W to $|\mathbf{b}|$ for $N = 6$ modes and a detector of radius $R = 4\pi$. For comparison, the equivalent response for a point-like detector and Zernike polynomials is also shown. The points and error bars represent the mean, 10th, and 90th percentiles from a sample of 100 random aberrations of a given magnitude. The graphs show that the function W depends predominantly on the length of the vector $\mathbf{b}$, indicating that W has the desired spherical symmetry.

For demonstration, the system was implemented experimentally by using a He–Ne laser (wavelength 633 nm) as the light source and a ferroelectric liquid-crystal spatial light modulator (SLM 256, Displaytech, Colorado) configured as a wavefront generator.[6] This acted as both aberration source and adaptive element, introducing a single aberration that was the sum of the input wave front and the adaptive element aberration. A CCD camera was used as the detector, and the spatial variation in sensitivity was implemented by the weighting of pixels within software.

To verify the performance of this system, the variation of output signal W with $|\mathbf{b}|$ was measured for $N = 6$ and $R = 4\pi$. The experimentally determined response, calculated as the mean value of W from ten random aberrations of a given magnitude, is shown in Fig. 1(b) and corresponds closely to the theoretical prediction.

For aberration correction, we followed the scheme employed in Ref. 1, in which a predetermined sequence of bias aberrations, represented by the vectors $\boldsymbol{\beta}_i$, was applied to the adaptive element, and the input aberration was then calculated from the resulting detector measurements. It was shown that the most efficient scheme for measuring N modes uses $\boldsymbol{\beta}_i$ that are the $N+1$ vertices of a regular N-dimensional simplex. A similar arrangement of biases was employed here. A random input aberration was introduced; this consisted of N LZ modes represented by the vector of coefficients $\mathbf{b}_{\mathrm{in}}$. The biases $\boldsymbol{\beta}_i$ were added in turn to the input aberration, giving the total

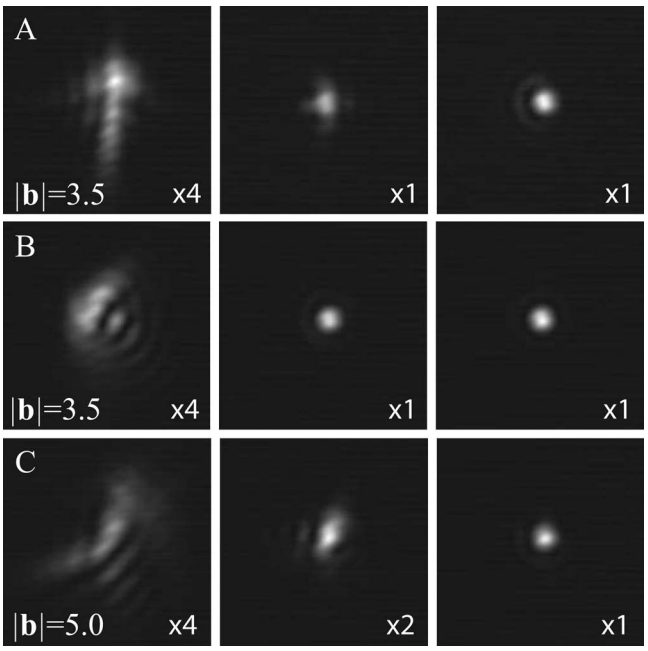

Fig. 2. Focal spot images before and after the measurement and correction cycles for three different starting aberrations. First column, initial aberrated spot; second column, after the first correction cycle; third column, after two correction cycles. The multiplication factor indicates the relative brightness of each spot image.

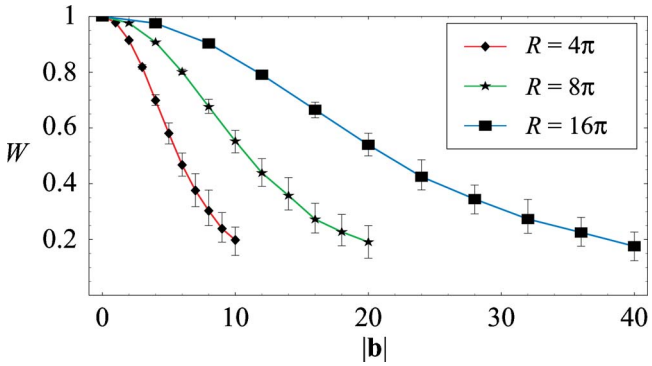

Fig. 3. (Color online) Variation of W with aberration magnitude $|\mathbf{b}|$ for detector radius R, showing the mean, 10th, and 90th percentiles from 100 random aberrations.

aberration $\mathbf{b}_{\text{in}}+\boldsymbol{\beta}_i$, and the corresponding detector measurements W_i were recorded. The measured aberration vector was then calculated as

$$\mathbf{b}_{\text{out}} = \mathbf{S}^{-1}(\mathbf{w} - \mathbf{w}_0), \tag{7}$$

where

$$\mathbf{w} = \left(\sum_{i=1}^{N+1} \boldsymbol{\beta}_i W_i\right) \Bigg/ \left(\sum_{i=1}^{N+1} W_i\right). \tag{8}$$

The vector $\mathbf{w}$ is independent of the overall intensity.[1] Equation (7) employs the diagonally dominated matrix $\mathbf{S}$, whose elements are defined as

$$S_{ik} = \frac{\partial W_i}{\partial b_k}, \tag{9}$$

and the small offset $\mathbf{w}_0=\mathbf{w}$, where both were calculated by using Eqs. (6)–(8), setting $\mathbf{b}_{\text{in}}=\mathbf{0}$. Note that $\mathbf{S}^{-1}$ and $\mathbf{w}_0$ are known in advance and do not require recalculation for each measurement. The measured aberration $\mathbf{b}_{\text{out}}$ was then subtracted from the input aberration. This process reduced the lateral aberration of the spot. If the resultant wavefront aberration was sufficiently small, a similar process could be followed using the Zernike series representation of the aberration and a small, pinhole detector function. This two-step process is illustrated in Fig. 2 for the correction of three different aberrations consisting of $N=6$ modes. The first column shows the initial focal spot with $|\mathbf{b}_{\text{in}}|=3.5$ (rows A and B) and $|\mathbf{b}_{\text{in}}|=5.0$ (row C). Correction of the lateral aberration by using LZ polynomials resulted in the spots shown in the second column. The third column shows the focal spot after correction of the wavefront aberration by using Zernike polynomials. Each correction cycle required only 7 detector measurements, giving 14 measurements in total. For the first correction cycle, a quadratically weighted detector of radius $R=4.0\pi$ and $|\boldsymbol{\beta}_i|=4.0$ were used. The second cycle used a circular uniform detector of radius $R=0.5\pi$ and $|\boldsymbol{\beta}_i|=0.7$. We note that in certain cases (e.g., row B) the aberration is almost fully corrected even after the first cycle.

Figure 3 shows results of calculations that demonstrate the variation of W with $|\mathbf{b}|$ for different detector radii. Since the scheme is based on a geometrical optics model, it can be easily adapted to deal with larger aberrations by using larger detector radii and correspondingly larger $|\boldsymbol{\beta}_i|$. For example, a doubling of the detector radius leads to a doubling of the width of the W response, an effect that is apparent in the figure. This scalability leads to the possibility of wavefront sensorless adaptive optics systems for arbitrarily large aberrations. The method can also be extended to deal with more modes. It is robust in the presence of additional modes if their combined amplitude is small; since the extra modes are orthogonal to those measured, W retains its spherical symmetry. If more modes are included in the correction procedure while the same $\boldsymbol{\beta}_i$ are used, the accuracy tends to decrease, particularly for larger values of $|\mathbf{b}_{\text{in}}|$. This can be rectified by employing a different biasing scheme using more bias aberrations.

M. J. Booth's e-mail address is martin.booth@eng.ox.ac.uk.

References

1. M. J. Booth, Opt. Express **14**, 1339 (2006).
2. M. Born and E. Wolf, *Principles of Optics*, 6th ed. (Pergamon, 1983).
3. R. Noll, J. Opt. Soc. Am. **66**, 207 (1976).
4. W. Lukosz, Opt. Acta **10**, 1 (1963).
5. J. Braat, J. Opt. Soc. Am. A **4**, 643 (1987).
6. M. A. A. Neil, M. J. Booth, and T. Wilson, Opt. Lett. **23**, 1849 (1998).